An *ab initio* study on stacking and stability of TiAl$_3$ phases

C.M. Fang*, Z. Fan

BCAST, Brunel University London, Uxbridge, Middlesex UB8 3PH, UK

ARTICLE INFO

ABSTRACT

TiAl$_3$ persists in many Al alloys and plays a detrimental role in solidification of related melts. Knowledge about TiAl$_3$ phases and phase relations is of importance to get some insight into the solidification processes, the microstructures and the properties of Al alloys. In this manuscript, we present a systematic study of the basic structures of TiAl$_3$ with aid from *ab initio* density functional theory (DFT) calculations. The study confirms that the ground state of TiAl$_3$ has the D0$_{23}$ structure, whereas the observed D0$_{22}$ type is a metastable phase. The calculations have identified the stability of a series of stacking composed of both D0$_{22}$- and D0$_{23}$-TiAl$_3$ units. At elevated temperature, the equilibrium configuration contains neither pure D0$_{23}$ nor pure D0$_{22}$ but will consist of a combination of the TiAl$_3$ cubes arranged to minimise its Gibbs energy. Stacking default investigation reveals a large energy barrier for the D0$_{22} \leftrightarrow$ D0$_{23}$ transition. The obtained information sheds some light on the rich variety of the experimental observations in Al alloys, and further to understand the complex titanium aluminides and their thermo-structural properties.

1. Introduction

TiAl$_3$ has been a topic of intensive research due to its rich variety of phases, unique structures and industrial applications. This compound plays an important role in heterogeneous nucleation of Al alloys [1–5]. TiAl$_3$ acts as a grain refiner independently [2,3] or co-plays with TiB$_2$ in the widely used Al-5Ti-B or Al-3Ti-B master alloys [4]. Recently high resolution transmission electron microscopy (HRTEM) observations revealed the formation of one most-likely TiAl$_3$ atomic layer at the TiB$_2$ substrate in Al. This two dimensional compound (2DC) of TiAl$_3$ structure plays a crucial role in the solidification of Al alloys [5,6]. Moreover, TiAl$_3$ can be formed at Ti-Al interfaces during thermal treatments for Al alloy welding [7,8]. This indicates the importance of developing some understanding about the compound for industrial applications. Ti-Al compounds including TiAl$_3$ and their phase relations have been a subject of extensive investigations, probably just second only to the Fe-C system [9–15]. Recently, Batalu and co-workers analysed and re-evaluated the Ti-Al binary phase diagram and showed that there is no phase transition for the TiAl$_3$ (probably D0$_{22}$ structure) up to its peritectic point [9]. Schuster and Palm showed a low-temperature (LT) to a high temperature (HT) phase transition for TiAl$_3$ but without a clear transition temperature [10]. In other binary phase diagrams, a LT-HT transition occurs at 735 °C [11,12] or at about 600 °C [13–15]. There have been experimental reports on the rich variety of structures of different lengths of *c*-axis and variation of corresponding *a*-axis of the

(D0$_{22}$-)TiAl$_3$ (Table 1) [7–28]. By sintering of elemental powders, Nakayama and Mabuchi obtained the cubic L1$_2$-TiAl$_3$ phase which contains some transition metal elements [7,26]. Further experiments confirmed that the L1$_2$-TiAl$_3$ phase is stabilized by impurities [27–29]. To get some insight into the relations for the TiAl$_3$ phases, theoretical methods have been employed for TiAl$_3$ [30–42]. The early first-principles simulations employed the local density functional approximation (LDA) [30–34] for the known structures and demonstrated the high stability of the D0$_{22}$-type structure [32]. Based on the available experimental values and *ab initio* calculations, Zope and Mishin built interatomic potentials for (large-scale) atomistic simulations of the Ti-Al system [36]. Using full-potential linear muffin-Tin orbital (PF-LMTO) method, Amador and co-workers investigated the influence of atomic stackings and atomic displacements from the ideal positions and revealed that the D0$_{23}$-phase is the ground state [30]. This conclusion was confirmed later by other calculations using various first-principles density-functionals [37–44] (Table 1). Zhang and Wang investigated the lattice vibration contribution to the relative stability of Ti-Al compounds, including the TiAl$_3$ phases [43]. They concluded that lattice vibration contribution doesn't change the stability order of the TiAl$_3$ phases. This is understandable since all the TiAl$_3$ phases have similar local coordination and chemical bonding. Tang and co-workers performed first-principles calculations for some one-dimensional long period structures (1D-LPSs) based on the cubic L1$_2$-TiAl$_3$ [45,46]. In the present manuscript, we have analysed systematically the existing TiAl$_3$

---

* Corresponding author.
  E-mail address: changming.fang@brunel.ac.uk (C.M. Fang).

Table 1
Calculated results (lattice symmetry (lat. sym.) and space group (S.G.); fractional atomic coordinates; and energy differences with respect to the formation energy of the cubic $L1_2$-$TiAl_3$ at 0 K (Eq. (1)). n in column one represent the number of stacking layers. The schematic structures are shown in Fig. 1.

Phase (n)	Lat. sym./S.G.	Lat. Para. (Å)	ΔE_1 (eV/TiAl$_3$)	Method and references
$L1_2$ (n = 1) Fig. 1a/1b	Cubic, Pm-3 m (No. 221)	$a = 3.977$	0.0	DFT-PBE this work
		$a = 3.960$	0.0	HSE(PBE0) this work
		Previous DFT calc.		
		$a = 3.97$	0.0	FP_LMTO [30]
		$a = 3.908$		DFT-LDA [62]
		$a = 3.91$		DFT-LDA [38]
		$a = 3.8997$		DFT-LDA [44]
		$a = 3.9854$		DFT-GGA [44]
		$a = 3.981$	0.0	DFT-GGA [40]
		$a = 3.978$		DFT-GGA [62]
		$a = 3.9779$	0.0	DFT-GGA [25]
		$a = 3.9824$		DFT-GGA [27]
		$a = 3.977$		DFT-GGA [39]
		Experimental data		
		$a = 3.967$		[42]
		$a = 3.967$–4.05		[37]]
$D0_{22}$ (n = 2) Fig. 1c	Tet.I4/mmm (No. 139)	$a = 3.841$, $c = 8.618$	−0.108	DFT-PBE this work
		$a = 3.826$, $c = 8.571$	−0.120	HSE(PBE0) this work
		Previous DFT calc.		
		$a = 3.76$, $c = 8.50$	−0.091	FP_LMTO [30]
		$a = 3.847$, $c = 8.656$		DFT-LDA [35]
		$a = 3.79$, $c = 8.45$		DFT-LDA [38]
		$a = 3.7678$, $c = 8.4818$		DFT-LDA [44]
		$a = 3.8507$, $c = 8.6332$		DFT-GGA [44]
		$a = 3.847$, $c = 8.621$		DFT-GGA [46]
		$a = 3.843$, $c = 8.616$	−0.112	DFT-GGA [40]
		$a = 3.8399$, $c = 8.6399$	−0.096	[30]
		Experimental data		[38]
		$a = 3.849$, $c = 8.610$		[19,20]
		$a = 3.847^*$, $c = 8.585$		[23]
		$a = 3.851$, $c = 8.612$		[42]
		$a = 3.836$, $c = 8.5791$		[63]
		$a = 3.846$, $c = 8.521$		[64]
		$a = 3.8537$, $c = 8.5839$		[65]
		$a = 3.849$, $c = 8.610$		[67]
		$a = 3.8537$, $c = 8.5839$		[65]
N113 (n = 3) Fig. 1e	Tet.P4/mmm (No. 123)	$a = 3.881$, $c = 12.604$	−0.124	DFT-GGA, this work
$D0_{23}$ (n = 4) Fig. 1d	Tet.I4/mmm (No. 139)	$a = 3.895$, $c = 16.662$	**−0.131**	DFT-PBE this work
		$a = 3.877$, $c = 16.595$	**−0.159**	HSE(PBE0) this work
		Previous DFT calc.		
		$a = 3.81$, $c = 16.44$	**−0.101**	FP_LMTO [30]
		$a = 3.8962$, $c = 16.6713$	**−0.127**	DFT-GGA[40]
		$a = 3.891$, $c = 16.924$		DFT-GGA[42]
		Experimental data		
		$a = 3.947$, $c = 16.679$		[25,67]
		$a = 3.890$, $c = 16.824$		[42]
		$a = 3.875$, $c = 16.916$		[19]
$D0_{19}$	Hex.P6$_3$/mmm (No. 194)	$a = 5.566$	+0.203	
		$c = 4.724$		

phases and predicted various stackings by application of the one-dimensional antiphase domain (1d-APD) model [19–23,47] based on the $D0_{22}$ structure using *ab initio* density functional theory (DFT). We also performed DFT calculations with hybrid-functional correction for the three known $TiAl_3$ ($L1_2$, $D0_{22}$ and $D0_{23}$) phases. Our calculations have confirmed that the ground state $TiAl_3$ has the $D0_{23}$-type structure. The study also revealed a series of highly stable structures containing $D0_{22}$ and $D0_{23}$ components. Symmetry analysis was performed for the obtained structures of high stability. The present study suggests that many experimental observations are the 'averaged structure' of a complex series of $TiAl_3$ structures. The obtained information can serve to characterize the $TiAl_3$ structures in Al alloys, to understand other titanium aluminides in the $TiAl$-$TiAl_3$ partial system, and to other intermetallic systems, as well; and further to analyse the two-dimensional compounds (2DC) formed at the substrates during heterogeneous nucleation [4–6].

2. Calculational details

In this study we employed the plane wave method in the Projector Augmented-Wave (PAW) framework which has been implemented in the Vienna *Ab initio* Simulations Package (VASP) [48–51]. The exchange and correlation terms were described using the Generalized Gradient Approximation (GGA) formulations by Perdew, Burke and Ernzerhof (PBE) [52]. It has been well-established that the GGA approximation describes better the 3d transition metals (Ti in this case) and their compounds [52–54]. The cut-off energies for the wave functions and for the augmentation functions were 550 eV and 700 eV, respectively. These values are higher than the default values, 178.330 eV and 328.883 eV for Ti; and 240.300 eV and 291.052 eV for Al. This serves to get high accurate valence-electrons' energies. The electronic wave functions were sampled on very dense grids, in the irreducible Brillouin zone (BZ) for the crystals, e.g. $20 \times 20 \times 20$ grid (220 k-points) for the cubic $L1_2$-$TiAl_3$ unit cell, using the Monkhorst and Pack

method [55]. The k-meshes of the related TiAl$_3$ structures were adjusted according to its unit cells. Tests of k-meshes from $16 \times 16 \times 16$ (120 k-points) up to $32 \times 32 \times 32$ (816 k-points) and cut-off energies for the cubic cell showed a good energy convergence (< 1 meV/atom). Both lattice parameters and coordinates of atoms are fully relaxed.

3. Calculated results and discussions

We first performed calculations for the related elemental solids, face-centred cubic (fcc) Al and hexagonal close-packing (hcp) α-Ti using the settings mentioned before. The obtained ground-state lattice parameters are compared with the experimental data (in parenthesis): $a = 4.0397$ (4.0495) Å for Al, $a = 2.9236$ (2.9508) and $c = 4.6259$ (4.6855) Å for α-Ti [56]. Clearly, the theoretical calculations reproduced the experimental values within 1.3%. Such excellent agreement confirms the reliability of our settings.

3.1. Basic structures of TiAl$_3$

We first present the calculated results for the known TiAl$_3$ structures and make a comparison between the present theoretical results with the experimental observations and previous theoretical studies available in the literature in Table 1 which also includes the calculated results using the hybrid-functional method (HSE) [57], a 'beyond DFT' approach which provides better descriptions for transition metals and other materials [57–59]. The employed parameters include the mixing coefficient α = 0.15 and the screen coefficient ω = 0.20 [60].

As shown in Table 1, the advanced HSE calculations confirmed the DFT results. The HSE lattice parameters are just slightly smaller than the corresponding DFT-GGA results and the calculated energies differences are in line with each other. This behaviour agrees with former comparative calculations using the DFT-GGA and the hybrid-functional (HSE) approximations [60,61]. Overall, our present calculations reproduced the experimental data (about 1%) and agree well with the previous calculations.

Table 1 lists the calculated energy differences of D0$_{22}$-, D0$_{23}$-, and D0$_{19}$-TiAl$_3$ with respect to the cubic L1$_2$ phase. Clearly the D0$_{22}$- and D0$_{23}$-TiAl$_3$ phases are more stable, whereas the D0$_{19}$-phase is notably less stable and will not be discussed further. The stability order for the known compounds is D0$_{23}$ > D0$_{22}$ > L1$_2$ from both the DFT-GGA and the hybrid-functional calculations (Table 1). Therefore, the ground state TiAl$_3$ has the D0$_{23}$-type structure rather than the widely observed D0$_{22}$-type. This agrees with the former theoretical studies, as well. This discrepancy between the *ab initio* calculations and observations will be rationalized in detail in the following sections. The calculations also showed that the energy difference between D0$_{23}$-type and D0$_{22}$-type is 23 meV/f.u. or 8 meV/atom from the DFT-GGA calculations or 39 meV/f.u. or 10 meV/atom from the hybrid-functional calculation. The cubic L1$_2$-type is metastable, which agrees with the experimental observations that the presence of impurities is necessary to stabilize it [26–28].

Using the L1$_2$-TiAl$_3$ as unit, we can build different TiAl$_3$ stackings. There are two ways to arrange the position of the Ti atoms: one is at the origin of the cube (named A, Fig. 1a), and other at the bottom centre of the cube (B, Fig. 1b). There are various ways to stack n cubes on each other along the c-axis with the A and B cubes. As shown in Fig. 1c, the D0$_{22}$ structure has an alternative A (at the origin) and B (at the centre of the cell) stacking, /AB/; whereas the D0$_{23}$ has alternative stacking of both /AA/ and /BB/ pairs (Fig. 1e). The N113 has both one /AA/ pair and /AB/ stacking (Fig. 1d).

It is also interesting to notice that the N113 structure (Fig. 1d) has very high stability and its formation energy close to that of the ground state D0$_{23}$ with a small difference of 7 meV/f.u. or 2 meV/atom from the DFT-GGA calculations. The structure of the N113 is also rather unique: it can be regarded either a combination of a /B/ in the A chain or a separated /AA/ pair.

Here we compare the calculated formation energies of the phases

with respect to the elemental solids (fcc-Al and hcp-Ti) using the formula $\Delta E_0(\mathrm{TiAl_3}) = \{E(\mathrm{TiAl_3}) - [E(\mathrm{Ti}) + 3\ E(\mathrm{Al})]\}/4$ in the unit eV/atom for the widely known D0$_{22}$-TiAl$_3$ with the experimental measurements in the literature. Our DFT-GGA calculations provide −0.403 eV/atom (−38.88 kJ/mol) for D0$_{23}$-TiAl$_3$, −0.397 eV/atom (−38.30 kJ/mol) for D0$_{22}$-TiAl$_3$, and −0.370 eV/atom (−35.72 kJ/mol) for L1$_2$-TiAl$_3$. Here we use both eV/atom and kJ/mol (1eV/atom = 96.4869 kJ/mol) for the reader's convenience. Rzyman and co-workers measured the formation enthalpy for (D0$_{22}$-)TiAl$_3$ using different techniques and obtained a group of data ranging from −35.7 to −39.6 kJ/mol [66]. Our calculated value for the D0$_{22}$-TiAl$_3$ (38.30 kJ/mol) is in the experimental range.

Here we have a close look at the lattices of the basic structures. Among the D0$_{22}$-, D0$_{23}$- and N113 phases (Fig. 1), D0$_{22}$-TiAl$_3$ has the shortest a-axis and longest c-axis per formula unit, meanwhile D0$_{23}$-TiAl$_3$ has the longest a-axis and shortest c-axis per formula unit. The axis lengths of the N113 phase are in-between. Structural analysis showed that the fractional coordinates of atoms are in the ideal sites for the D0$_{22}$-TiAl$_3$, whereas the z-components of atomic coordinates deviate from their ideal positions in the N113 and D0$_{23}$-TiAl$_3$ phases (Table 1). There are Ti-Ti pairs of interatomic distances of about 3.935 Å in N113 and 3.972 Å in D0$_{23}$-TiAl$_3$ along their [0 0 1] orientation. These distances of the Ti-Ti pairs are notably smaller than those of the averaged interlayer distances (4.201 Å for N113 and 4.185 Å for D0$_{23}$-TiAl$_3$). As a consequence, both Al atoms and Ti atoms deviate slightly from their plane, as shown in Fig. 1d and e.

3.2. Effects of one /B/ or one /BB/ pair in the L1$_2$-TiAl$_3$ chains

Before addressing the stability and structural properties of various stacking of TiAl$_3$ cubes in a systematic way, we investigate the effects of one /B/ or one /BB/ pair in the A-chains [A$_n$] of different lengths (up to $n = 12$). The energy differences of the structures with respect to that of the cubic L1$_2$ are defined as:

$$\Delta E_1 = [E(n\mathrm{TiAl_3}) - nE(\mathrm{L1_2 - TiAl_3})]/n \tag{1}$$

Similarly, the variations of the lattice parameters are also defined as

$$\Delta a = a(n\mathrm{TiAl_3}) - a_0(\mathrm{L1_2 - TiAl_3}) \tag{2}$$

$$\Delta c_1 = [c(n\mathrm{TiAl_3}) - na_0(\mathrm{L1_2 - TiAl_3})]/n \tag{3}$$

where $E(n\mathrm{TiAl_3})$, $a(n\mathrm{TiAl_3})$, $c(n\mathrm{TiAl_3})$ and the calculated total valence electron energy, the length of a-axis and the c-axis for $n\mathrm{TiAl_3}$, respectively. And $E(\mathrm{L1_2-TiAl_3})$ and $a_0(\mathrm{L1_2-TiAl_3})$ are the energy and length of a-axis for L1$_2$-TiAl$_3$. ΔE_1 and Δc_1 are normalized to per TiAl$_3$ unit. The calculated results are shown in Fig. 2.

Clearly for one /B/ in the [A$_n$] chain (Fig. 2a for $n = 6$ as an example), the most stable configuration with respect to L1$_2$-TiAl$_3$, is $n = 2$, that is the D0$_{22}$ structure. With increasing n, the energy difference (ΔE) increases or in other words the stability becomes lower. Fig. 2c also shows the dependence of ΔE on the chain length (n) for the structures with one /BB/ pair in the [A$_n$] chain (e.g. Fig. 2b for $n = 6$). The most stable structure is for $n = 4$, the D0$_{23}$ structure. With increase of n, ΔE increases. As n approaches infinity, the energy differences and length differences of the axis will become zero, as the crystals become the cubic L1$_2$ structure.

3.3. High index stacking series

The energetics of TiAl$_3$ structures of higher stacking numbers based on the D0$_{22}$- and D0$_{23}$- structure was investigated. The calculated formation energies with respect to the cubic L1$_2$-TiAl$_3$ are shown in Fig. 3. Here we report our analysis of the symmetry and related stability.

For stacking number n = even, the D0$_{22}$-based structures can be regarded as just supercells of the basic structure with formula [AB]$_n$, Therefore, there is no change of symmetry and space group. For
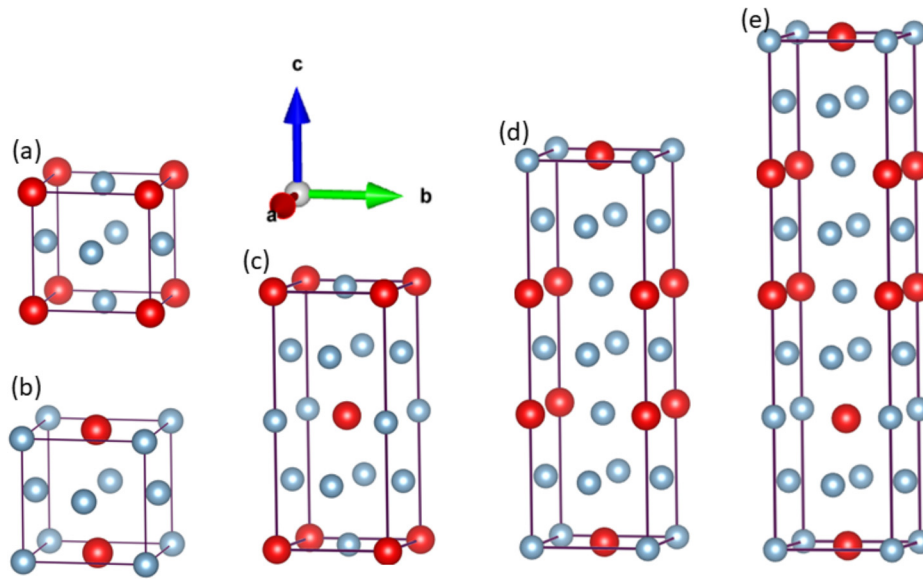
Fig. 1. Schematic structures for (a) cubic L1$_2$-TiAl$_3$ with A-stacking (Ti at origin), (b) cubic L1$_2$-TiAl$_3$ with B-stacking (Ti at body center); (c) tetragonal D0$_{22}$-TiAl$_3$, (d) tetragonal N11, and (e) tetragonal D0$_{23}$-TiAl$_3$ (see Table 1).

n = odd, the D0$_{22}$-based structure contains one /BB/ or /AA/ stack. This causes the lowering of the energy of the supercell in Fig. 3. With increasing n value, ΔE increases, and approaches that of the D0$_{22}$-TiAl$_3$ when n is large enough. This behaviour is understandable because of the decreasing effect of the /BB/ unit in the whole unit cell.

Symmetry analysis showed that for n = odd, the D0$_{22}$-based TiAl$_3$ lattices are still tetragonal. Their space group is P4/mmm (No. 123) lower than the I4/mmm (No. 139) for the D0$_{22}$-TiAl$_3$ because of the loss of an internal translation symmetry (body centre operation). The simplest example is the N113 phase (Table 1). The structures for n = odd have distorted lattices with shorter Ti-Ti distances (~3.95 to 3.98 Å) along the c-axis.

The energetics for the D0$_{23}$-based structures displays different behaviour from that of D0$_{22}$-based structures, as shown in Fig. 3. Their behaviour can be described as follows:

(a) For n = 4m (m = 1, 2, 3 …), the structures are supercells of the primitive D0$_{23}$–TiAl$_3$, the ground state with space group I4/mmm (No. 139). There are Ti-Ti pairs with interatomic distances in the range of 3.95 to 3.98 Å.

(b) For n = 4m + 1 (m = 1, 2, 3 …), each D0$_{23}$–based structure contains three unpaired TiAl$_3$ units. The space group of this family is still P4/mmm (No. 123) as shown for the simplest case n = 5 which contains one /AA/ pair continued by a /BAB/ series. The formation energies of this family are notably higher than that of the ground state, but decrease with increase of n.

(c) For n = 4m + 2 (m = 1, 2, 3…), each D0$_{23}$–based structure contains two unpaired TiAl$_3$ units. The space group of this family can
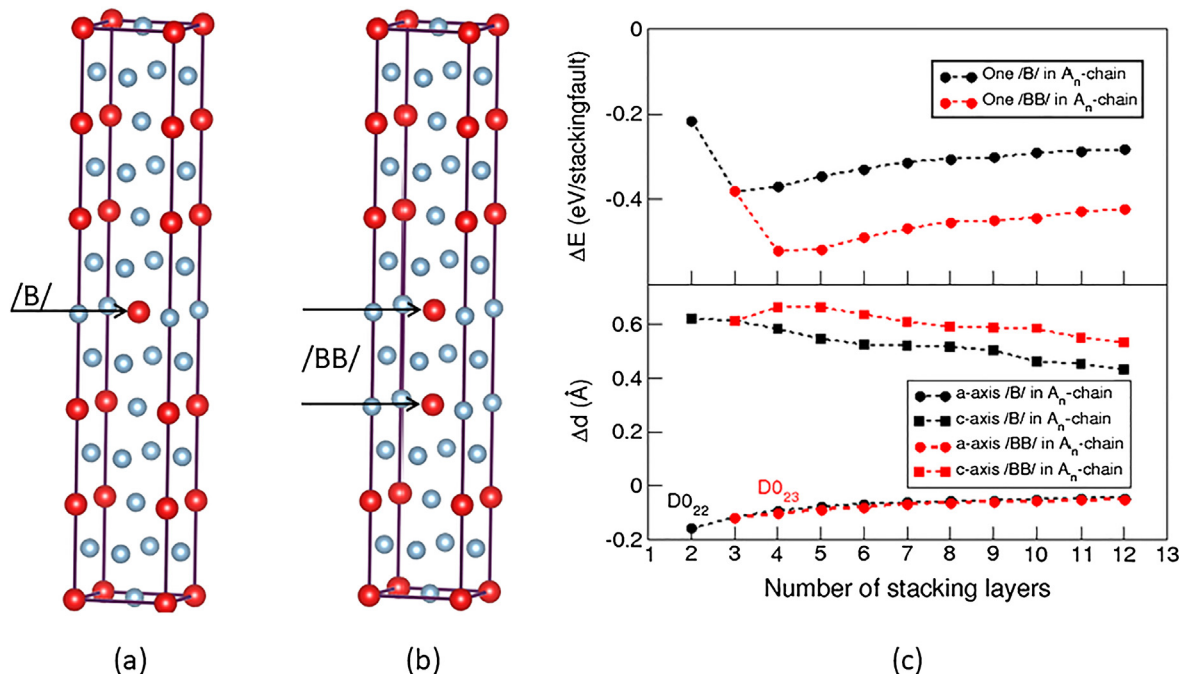
Fig. 2. Schematic structures for (a) a /B/ in one [A$_n$] chain (n = 6), and (b) a /BB/ in one [A$_n$] chain (n = 6). (c) The dependences of the energy difference, ΔE_1 (Eq. (1)) and the differences of the axis lengths Δa and Δc_1 (Eqs. (2) and (3)) on the stacking number n.
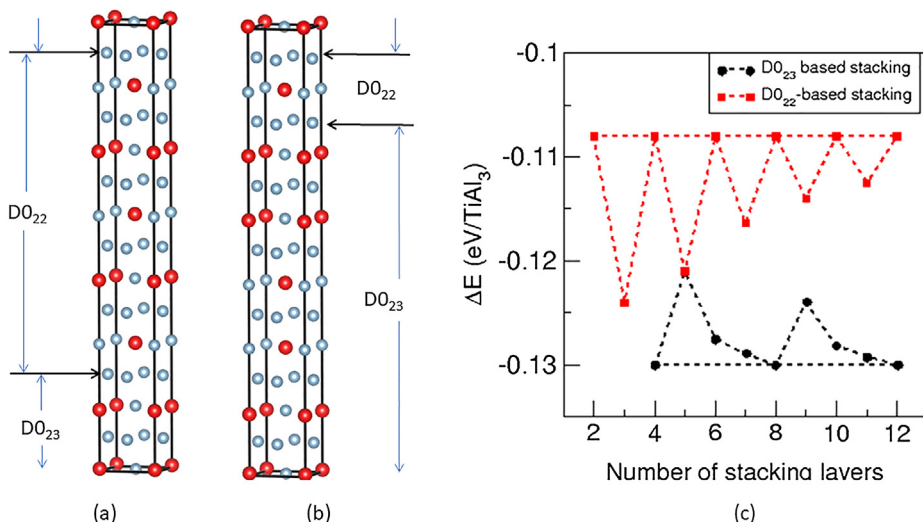
Fig. 3. Schematic structures for (a) one $D0_{23}$ unit in a $D0_{22}$ chain (n = 7, as an example), and (b) one $D0_{22}$ in a $D0_{23}$ chain (n = 7). (c) The calculated energy difference of the stacking with respective to the cubic $L1_2$-$TiAl_3$ (Eq. (1)). The red squares represent the stacking based on $D0_{22}$-type, the black spheres on $D0_{23}$-type structure. The dotted lines are used to guide readers' eyes.

be lowered to P4/mm (No. 99). Their formation energies are between the corresponding structure with $n = 4m + 1$ and the ground state as shown in Fig. 3. However, if $n = 3m$, this stacking can be supercells of the N113. Then the space group is P4/mmm (No. 123).

(d) For $n = 4m + 3$ (m = 1, 2, 3…), each $D0_{23}$–based structure contains just one unpaired $TiAl_3$ unit. This structure can be also regarded as $n = 4m − 1$ (m = 2, 3, 4…). The space group of this family is lowered to P4/mmm (No. 123). Their formation energies are quite close to that of the ground state as shown in Fig. 3.

Overall when n is large enough, the formation energy of the n stacking approaches that of the ground state, $D0_{23}$-TiAl.

4. Discussions: 1d-APD in $D0_{22}$-$TiAl_3$ chain and configuration entropy

Here we address the discrepancy between the *ab initio* calculations and the experimental observations that the *ab initio* density-functional theory (DFT) calculations provided that $D0_{23}$-$TiAl_3$ is the ground state, while most experimental observations indicated that the observed structure is the $D0_{22}$-$TiAl_3$ phase.

As shown before, the $D0_{23}$- and $D0_{22}$-$TiAl_3$ are both consequences of stacking of the $TiAl_3$ alternative units. Experiments revealed that variation of unit lattices and c/a ratios from the prepared samples [8–28]. By means of mechanical and thermal treatments, Lee and co-workers obtained several $TiAl_3$ structures, including $D0_{23}$- at low temperature (400–600 °C) and a Ti_8Al_{24} with the c'/a (c' is $c/8$) (=1.0922) being in-between those of $D0_{22}$-phase (1.0624) and $D0_{23}$- phase (1.1184). In fact the measured $D0_{23}$-$TiAl_3$ from their samples has a c'/a value (1.0742) which is slightly larger than that of the sample at 600 °C [25]. This indicates dependence of stacking on temperature.

As shown in Fig. 3, the structure of $TiAl_3$ depends on its stacking number. It is also noted that the energy difference between $D0_{22}$- and $D0_{23}$-$TiAl_3$ is quite moderate (Table 1 and Fig. 3). In fact these two structures can be regarded as differences in stackings. For example, for the basic $D0_{23}$-$TiAl_3$ structure can be considered as a Burger's stacking fault operation, that is to move half of the unit cell from (0,0) to (1/2,1/2) on a supercell (double c-axis) of $D0_{22}$-$TiAl_3$. This corresponds to the fact that for $D0_{22}$-$TiAl_3$ with an odd stacking number, there is always a /BB/ pair and therefore, an extra freedom $w = (n − 1)$. The configurational entropy is $S = k_B \ln w$ (here k_B is the Boltzmann constant) or $S = [k_B \ln(n − 1)]/4n$ per atom. This indicates that the configurational entropy will stabilize the $D0_{22}$-structure at elevated temperature and that the configurational entropy contribution decays with the number of stacking.

Here we discuss the impact of extra freedom on the 1d-APD in detail [19–23,47] to assess the stability of $D0_{22}$-$TiAl_3$ at elevated temperature, using $n = 8$ series as an example. Assuming that there is one 1d-APD in this configuration, then this structure has (a) an formation energy of about −0.070 eV/cell or −0.009 eV/$TiAl_3$ with respective to that of $D0_{22}$, (b) freedom of configurations, $w = 8$ due to the fact that such 1d-APD may occur for each $TiAl_3$ unit in the cell. Correspondingly, the configurational entropy is $S_{conf.} = k_B \ln w = 8.617 \times 10^{-5} \times 2.079$ eV/K = 0.1792 10^{-3} eV/K. For a temperature $T = 600$ K, the free energy change is $\Delta G(600 \text{ K}) = \Delta E - T S_{conf} = -0.070–0.118 = -0.188$ eV/cell or −23.5 meV/f.u. This value is larger than the enthalpy difference between $D0_{22}$- and $D0_{23}$-$TiAl_3$ from the DFT-GGA calculations (Table 1). That indicates the free energy of this $D0_{22}$-$TiAl_3$ series with one 1d-APD is lower than that of ground state, $D0_{23}$-$TiAl_3$. In other word, at or above 600 K the high-temperature phase containing more $D0_{22}$-$TiAl_3$ stacking is more stable than the ground $D0_{23}$-$TiAl_3$ structure.

To get some insight into the energy barriers for formation of an extra stacking or for an 1D-APD, we investigate the generalized stacking fault (gsf) energy using the structure of $n = 12$ as an example. The $n = 12$ may have different stacking: $D0_{22}$-(12 times), $D0_{23}$ (6 times) and the intermediate N113 (4 times). It may also contain two separated /BB/ pairs by shifting half of its unit cell (c-axis) along ⟨1 1 0⟩ from (0,0) to (1/2,1/2) in plane from the $D0_{22}$ structure as the starting configuration. The schematic structures and calculated energetics are shown in Fig. 4. The calculations showed that the energy increases with this shift and reaches a maximum at (0.25,0.25), then it decreases and finally reaches its minimum at (0.5,0.5). The energy barrier is about 2.2 eV (Fig. 4). Such higher energy barrier indicates that phase transformation can occur only at high temperature. This high energy barrier also indicates that at high temperature, once the $D0_{22}$-based stacking is formed, it requires a large driving force (e.g. temperature differences) and a long period of time to complete transitions to the ground state $D0_{23}$-$TiAl_3$. In other words, the phase transition from the high temperature phase of a $D0_{22}$-$TiAl_3$ dominated chain to the low temperature phase with the $D0_{23}$-$TiAl_3$ structure occurs slowly at lower temperatures, e.g. at room temperature. This agrees with the experimental observations of a variety of $TiAl_3$ structures [9–24].

5. Summary

Ab initio density-functional theory calculations have been performed for the $TiAl_3$ phases. The calculations confirmed that the $D0_{23}$-phase is the ground state, and the $D0_{22}$-$TiAl_3$ is a high temperature phase. The calculations also showed that there exist a series of intermediate
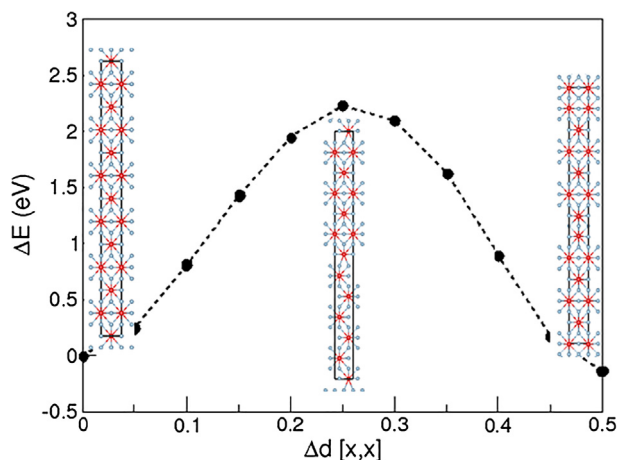
Fig. 4. The stacking fault energy for an cell of $n = 12$, starting from pure $D0_{22}$ stacking to one stacking with a $D0_{23}$ unit along the (0.0,0.0) to (0.5, 0.5) path. The dotted line is used to guide the readers' eyes.

stacking configurations of high stability. And there is a high energy barrier to form a new stacking. Therefore, the structures of $D0_{22}$ domains can be observed at low temperature. Depending on the preparation conditions and thermal history, the obtained samples contain various stacking of $TiAl_3$ units. The current experimental measurement techniques, such as X-ray diffraction, provide an 'averaged structure' of such a series of stackings. The information obtained in the present work is helpful to characterize the intermetallic compounds in the complex Al alloys. It is also worth mentioning that an understanding of the different $TiAl_3$ stacking is very useful to get insight into the crystal structures and phase-relations in the Ti-Al system, and related systems.

Acknowledgements

Authors' contributions

Dr. C. M. Fang: Initiated the research, performed all the calculations and wrote the manuscript.

Prof. Z. Fan: Motivated this study and wrote the manuscript.

References

[1] K.F. Kelton, A.L. Greer, Nucleation in Condensed Matter, Application in Materials and Biology, Pergamon Materials Series, Elsevier Ltd., Oxford/Amsterdam, 2010.
[2] G.S. Vinod Kumar, B.S. Murty, M. Chakraborty, J. Mater. Sci. 45 (2010) 2921.
[3] M. Easton, D. St John, Metall. Mater. Trans. A30 (1999) 1613.
[4] P. Schumacher, A.L. Greer, J. Worth, P.V. Evans, M.A. Kearns, P. Fisher, A.H. Green, Mater. Sci. Technol. 14 (1998) 394.
[5] Z. Fan, Y. Wang, Y. Zhang, T. Qin, X.R. Zhou, G.E. Thompson, T. Pennycook, T. Hashimoto, Acta Mater. 84 (2015) 292.
[6] Y. Wang, Z. P. Que, Y. Zhang, Z. Fan, in: Proceedings of the 6th Decennial International Conference on Solidification Processing, Beaumont Estate, Old Windsor, UK, 25–28 July 2017, p. 81.
[7] S.-J. Lee, H. Nakamura, Y. Kawahito, S. Katayama, Trans. JWRI 42 (2013) 17.
[8] F. Foadian, M. Soltanih, M. Adeli, M. Etminanbakhsh, Metall. Mater. Trans. B47 (2016) 2931.
[9] D. Batalu, G. Coşmeleaţă, A. Aloman, U.P.B. Sci. Bull. Ser. B68 (2006) 77.
[10] J.C. Schuster, M. Palm, J. Phase Equilib. Diffus. 27 (2006) 255.
[11] A. Grytsiv, P. Rogl, H. Schmidt, G. Giester, J. Phase. Equilib. 24 (2003) 511.
[12] V.T. Witusiewicz, A.A. Bondar, U. Hecht, S. Rex, T.Ya. Velikanova, J. Alloys Comp. 465 (2008) 64.
[13] J.L. Murray, Binary Alloys Phase Diagrams, in: T.G. Massalski (Ed.), ASM, Metals Park, Ohio, 1986, p. 173.
[14] C. MaCullough, J.J. Valencia, C.G. Levi, R. Mehrrabian, Acta Metall. 37 (1989) 1321.
[15] T.M. Radchenko, V.A. Tatarenko, H. Zapolsy, Solid State Phenomena 138 (2008) 283.
[16] A. Raman, K. Schubert, Z. Metallkunde 56 (1965) 44.
[17] A. Raman, K. Schubert, Z. Metallkunde 56 (1965) 99.
[18] E. Illeková, P. Švee, D. Janičkovič, J. Phys.: Conf. Series 144 (2009) 012111.
[19] F.J.J. van Loo, G.D. Rieck, Acta Metal. 21 (1973) 61.
[20] F.J.J. van Loo, G.D. Rieck, Acta Metal. 21 (1973) 73.
[21] J.H. Maas, G.F. Bastin, F.J.J. Van Loo, R. Metselaar, Z. Metallkunde 74 (1983) 294.
[22] R. Miida, M. Kasahara, D. Watanabe, Jpn. J. Appl. Phys. 18 (1980) L707.
[23] J.S. Shuster, H. Nowotny, C. Vaccaro, J. Solid State Chem. 32 (1980) 213.
[24] J.C. Schuster, H. Ipser, Z. Metalkunde 81 (1990) 389.
[25] H.M. Lee, J. Lee, Z.-H. Lee, Scripta Metal. 25 (1991) 517.
[26] N. Nakayama, H. Mabuchi, Intermetallics 1 (1993) 41.
[27] M.B. Winnicka, R.A. Varin, Metallurg. Trans. A24 (1993) 935.
[28] J.Q. Guo, K. Ohtera, K. Kita, T. Shibata, Mater. Sci. Eng. A181–182 (1994) 1397.
[29] K.E. Knipling, D.C. Dumand, D.B. Seidman, Acta Mater. 56 (2008) 1182.
[30] C. Amador, J.J. Hoyt, B.C. Chakoumakos, D. de Fontaine, Phys. Rev. Lett. 74 (1995) 4955.
[31] T. Hong, T.J. Watson-Yang, A.J. Freeman, T. Oguchi, J.-H. Xu, Phys. Rev. B 41 (1990) 12462.
[32] M. Asta, D. de Fontaine, M. van Schilfgaarde, M. Sluiter, M. Methfessel, Phys. Rev. B 46 (1992) 5055.
[33] M. Asta, D. de Fontaine, J. Mater. Res. 8 (1993) 2554.
[34] J. Zou, C.L. fu, M.H. Yoo, Intermetallics 3 (1995) 265.
[35] R.R. Zope, Y. Mishin, Phys. Rev. B 68 (2003) 024102.
[36] C. Colinet, A. Pastural, J. Phys. Condens. Matter 14 (2002) 6713.
[37] G. Ghosh, S. Vaynman, M. Asta, M.E. Fine, Intermetallics 15 (2007) 44.
[38] G. Bester, M. Fähnle, J. Phys.: Condens. Matter 13 (2001) 11551.
[39] Z.L. Chen, H.M. Zou, F.M. Yu, J. Zou, J. Phys. Chem. Solids 71 (2010) 946.
[40] H. Hu, X.Z. Wu, R. Wang, Z.H. Jia, W.G. Li, Q. Liu, J. Alloys Comp. 666 (2016) 185.
[41] G. Ghosh, M. Asta, Acta Mater. 53 (2005) 3225.
[42] S. Srinivasan, P.B. Desch, R.B. Schwarz, Scripta Metall. Mater. 125 (1991) 2513.
[43] H. Zhang, S.Q. Wang, J. Mater. Sci. Technol. 26 (2010) 1071.
[44] J. Li, M. Zhang, X. Luo, J. Alloys Comp. 556 (2013) 214.
[45] P.-Y. Tang, J.-Y. Li, G.-H. Huang, Q.-L. Xie, Comput. Mater. Sci. 91 (2014) 153.
[46] P.-Y. Tang, B.-Y. Tang, Solid State Commun. 152 (2012) 1939.
[47] C.H. Johansson, J.O. Linde, Ann. Phys. (Leipzig) 25 (1936) 1.
[48] G. Kresse, J. Hafner, Phys. Rev. B 49 (1994) 14251.
[49] G. Kresse, J. Furthmuller, J. Comput. Mater. Sci. 6 (1996) 15.
[50] P.E. Blöchl, Phys. Rev. B 50 (1994) 17953.
[51] G. Kresse, J. Joubert, Phys. Rev. B 59 (1999) 1758.
[52] J.P. Perdew, K. Burke, M. Ernzerhof, Phys. Rev. Lett. 77 (1996) 3865.
[53] C. Amador, R.L.W.L. Lambrecht, B. Segall, Phys. Rev. B 46 (1992) 1870(R).
[54] C.M. Fang, M.A. van Huis, M.F.H. Sluiter, H. Zandbergen, Acta Mater. 58 (2010) 2968.
[55] H.J. Monkhorst, J.D. Pack, Phys. Rev. B 13 (1976) 5188.
[56] R.W.G. Wyckoff, Crystal Structures, John Wiley, New York, 1963.
[57] J. Heyd, G.E. Scuseria, M. Ernzerhof, J. Chem. Phys. 118 (2003) 8207.
[58] A.D. Becke, J. Chem. Phys. 98 (1993) 1372.
[59] J.P. Perdew, M. Ernzerhof, K. Burke, J. Chem. Phys. 105 (1996) 9982.
[60] C.M. Fang, K. Biswas, J. Phys. Chem. C 120 (2016) 1225.
[61] C.M. Fang, K. Biswas, Phys. Rev. Appl. 4 (61) 014012.
[62] A.R. Boulechfar, S. Gemid, H. Meraji, B. Bouhafs, Physica B Condens. Matter 405 (2010) 4045.
[63] G. Brauer, Z. Anorg, Allg. Chem. 242 (1950) 1.
[64] P. Wodniecki, A. Kulinska, B. Wodniecka, J. Belosevic-Cavor, V. Koteski, J. Alloys Comp. 479 (2009) 56.
[65] P. Norby, A.N. Christensen, Acta Chemica Scand. A40 (1986) 157.
[66] K. Rzyman, Z. Moser, J.-C. Gachon, Arch. Metall. Mater. 49 (2004) 545.
[67] S.Z. Han, S.I. Park, J.-S. Huh, Z.-H. Lee, H.M. Lee, Mater. Sci. Eng. A 230 (1997) 100.